Contrasting fates of terrestrial organic carbon pools in marginal sea sediments

Author(s):
Yu, Meng; Eglinton, Timothy I.; Haghipour, Negar; Montluçon, Daniel B.; Wacker, Lukas; Hou, Pengfei; Ding, Yang; Zhao, Meixun

Publication date:
2021-09-15

Permanent link:
https://doi.org/10.3929/ethz-b-000495603

Originally published in:
Geochimica et Cosmochimica Acta 309, https://doi.org/10.1016/j.gca.2021.06.018

Funding acknowledgement:
163162 - Climate and Anthropogenic PerturbationS of Land-Ocean Carbon tracKs (CAPS-LOCK2) (SNF)
184865 - Climate and Anthropogenetic PertubationS of Land-Ocean Carbon tracKs (CAPS-LOCK3) (SNF)

Available online at www.sciencedirect.com

ScienceDirect

Geochimica et Cosmochimica Acta 309 (2021) 16–30

Geochimica et Cosmochimica Acta

www.elsevier.com/locate/gca

Contrasting fates of terrestrial organic carbon pools in marginal sea sediments

Meng Yu [a,b,c], Timothy I. Eglinton [c,*], Negar Haghipour [c], Daniel B. Montluçon [c], Lukas Wacker [d], Pengfei Hou [a,c], Yang Ding [a,b], Meixun Zhao [a,b,*]

[a] Frontiers Science Center for Deep Ocean Multispheres and Earth System, and Key Laboratory of Marine Chemistry Theory and Technology, Ministry of Education, Ocean University of China, Qingdao 266100, China

[b] Laboratory for Marine Ecology and Environmental Science, Qingdao National Laboratory for Marine Science and Technology, Qingdao 266237, China

[c] Geological Institute, Department of Earth Sciences, ETH Zürich, 8092 Zürich, Switzerland

[d] Laboratory for Ion Beam Physics, Department of Physics, ETH Zürich, 8093 Zürich, Switzerland

Received 19 October 2020; accepted in revised form 15 June 2021; Available online 20 June 2021

Abstract

Burial of terrestrial organic carbon (OC_{terr}) in marginal sea sediments is a key component of the carbon cycle, exerting long-term influence on atmospheric CO_2 and climate. Assessment of the burial efficiency of OC_{terr} is of key importance, yet remains poorly constrained due to current gaps in our knowledge of mechanistic controls, including the influence of organic matter composition and age on the fate of OC_{terr} in marine sediments. We measured bulk characteristics ($\delta^{13}C$ and $\Delta^{14}C$ of OC; mineral surface area, SA; grain size; $n = 98$ samples) and biomarker carbon isotopic compositions (fatty acid $\delta^{13}C$ and $\Delta^{14}C$; $n = 11$) of a suite of surface sediment samples from the Bohai Sea and Yellow Sea (BS-YS). Combining with published results, bulk OC ($n = 234$) and biomarker ($n = 19$) carbon isotopic data are used to examine spatial variability in the sources and ages of OC_{terr} in this shallow marginal sea system. Biomarker carbon isotopic values are used to constrain endmember values, and a dual carbon isotope mixing model was applied to all bulk samples to develop a spatially explicit assessment of contributions of different pools of OC_{terr}. Although highly spatially variable, pre-aged OC ($OC_{pre\text{-}aged}$) and fossil OC (OC_{fossil}) when combined (i.e., "non-modern OC") on average accounted for 51 ± 10% of the OC in BS-YS surface sediments. This was equivalent to the proportion of OC_{terr} (ave., 51 ± 14%) estimated from a $\delta^{13}C_{OC}$ binary mixing model, suggesting OC_{terr} in the mixed layer of BS-YS sediments is predominantly composed of millennial-aged OC. The burial potential of pool-specific OC_{terr} was then evaluated through comparison of corresponding mineral SA-normalized loadings of surface sediments with those of Yellow River suspended particulate matter. Both the regression slope and the arithmetic mean value approaches reveal high burial potential for all terrestrial OC pools delivered by Yellow River, which is attributed to the aged and refractory nature of OC exported from the Yellow River. However, differing relationships of pool-specific OC_{terr} loadings between BS-YS and Yellow River sediments imply contrasting fates. In particular, we find that the burial potential of $OC_{pre\text{-}aged}$ is consistently greater than that of OC_{fossil}. This surprising observation suggests either enhanced degradation of OC_{fossil} during lateral transport (possibly as a consequence of different mineral associations and hydrodynamic sorting effects), or additional sources for $OC_{pre\text{-}aged}$, such as from small rivers or aerosol deposition. Overall, OC age, mineralogical composition and hydrological settings contribute to the complex patterns of OC residing in northern China marginal sea surface sediments. This novel molecular-isotopic approach reveals significant spatial variability in proportions, contents and burial potential among

* Corresponding authors at: Frontiers Science Center for Deep Ocean Multispheres and Earth System, and Key Laboratory of Marine Chemistry Theory and Technology, Ministry of Education, Ocean University of China, No. 238, Songling Road, Qingdao 266100, China (M. Zhao); Geological Institute, Department of Earth Sciences, ETH Zürich, 8092 Zürich, Switzerland (T.I. Eglinton).

E-mail addresses: timothy.eglinton@erdw.ethz.ch (T.I. Eglinton), maxzhao@ouc.edu.cn (M. Zhao).

https://doi.org/10.1016/j.gca.2021.06.018

terrestrial OC pools, and underlines the importance of considering organic matter age and composition in understanding and constraining the fate of OC_{terr} in marine sedimentary environments.

Keywords: Terrestrial organic carbon; Compound-specific isotopes (^{13}C and ^{14}C); Organic carbon loading; Burial potential; Marginal seas

1. INTRODUCTION

Marginal seas account for up to 90% of sedimentary organic carbon (OC) burial in the ocean (Hedges and Keil, 1995), forming a key component of the global carbon cycle. The balance between burial and oxidation of OC delivered to marine sediments influences the atmospheric CO_2 inventory on a range of timescales (Galy et al., 2015; Leithold et al., 2016; Bianchi et al., 2018). With respect to supply of terrestrial OC (OC_{terr}) to the ocean, variations in source, age and transport pathway may influence its burial in marine sediments (Burdige, 2005; Blair and Aller, 2012; Hilton et al., 2015; Hage et al., 2020). It is estimated that globally, only about one third of OC_{terr} exported by rivers is buried in marine sediments, with the remainder subject to remineralization (Burdige, 2005; Blair and Aller, 2012; Galy et al., 2015), thereby likely constituting a CO_2 source on (sub-)millennial timescales (Bröder et al., 2018). Anthropogenic activities have also perturbed regional and global carbon budgets, including enhanced mobilization and export of pre-aged OC from soils to the ocean as a consequence of land-use change (Bauer et al., 2013; Regnier et al., 2013; Butman et al., 2015). Understanding the fate of OC_{terr} in marginal seas is thus an important, yet challenging imperative given numerous uncertainties associated with its supply and fate. Accurate constraints on the nature and burial of OC_{terr} in marginal sea sediments are essential for developing robust carbon budgets and for predicting future carbon dynamics.

The burial efficiency of OC_{terr} has been estimated by comparing riverine export and sediment burial fluxes (Hedges and Keil, 1995), however this approach carries large uncertainties (Keil et al., 1997; Bauer et al., 2013). OC contents normalized to mineral-specific surface area (SA), or "OC loadings" (OC/SA ratios) provide an alternative means to assess burial efficiency of terrestrial OC (Keil et al., 1997). Here, the assumption is that mineral particles remain largely unaffected by fluvial export, and OC_{terr} is associated with and protected by mineral surfaces during export (Keil et al., 1994; Blair and Aller, 2012; Hemingway et al., 2019). Decreases in OC_{terr} loadings between riverine particles and marine sediments thus imply degradation prior to burial. Using the loading approach, the global average burial efficiency of OC_{terr} was estimated to be 22 ± 5% on continental margins (Burdige, 2005), but wide variations have been found among different depositional settings (Keil et al., 1997; Burdige, 2005; Galy et al., 2007).

The above approach is based on the use of bulk OC $\delta^{13}C$ to constrain the fraction of OC_{terr} in marine sediments, but does not account for variations in OC_{terr} composition, age and reactivity. For example, the fate of millennial-aged soil-derived and fossil bedrock (petrogenic) OC (Drenzek et al., 2007; French et al., 2018; Vonk et al., 2019) may differ from that of modern OC_{terr} (Hage et al., 2020). The radiocarbon composition of bulk OC and source-diagnostic biomarkers provides independent constraints on OC ages and sources in marine sediments (Eglinton et al., 1997; Drenzek et al., 2007; Griffith et al 2010; Feng et al., 2013; Tao et al., 2016). Normalizing the proportions of different aged OC constituents or different biomarkers to SA (i.e., pool-specific OC or biomolecular loadings, respectively) sheds light on the fate of specific OC_{terr} components. Previous studies adopting such approaches have revealed significant changes in loadings of different OC_{terr} constituents during riverine transport (Freymond et al., 2018), estuarine transport (Hou et al., 2020) and across-shelf transport (Bröder et al., 2018). However, a molecular isotope-based loading approach has not been systematically applied in marginal sea systems.

The eastern China marginal seas are a globally important continental shelf system, and are well-suited for investigations of the controls on OC_{terr} burial given their spatially heterogeneous nature in terms of OC sources and ages (Bao et al., 2016; van der Voort et al., 2018). OC burial in the eastern China marginal sea surface sediments (most samples are from the 0–3 cm) (13 Mt yr^{-1}) accounts for ~10% of global OC burial on continental margins (138 Mt yr^{-1}) (Burdige, 2005; Deng et al., 2006; Hu et al., 2016). OC_{terr} is mainly supplied by the Yellow River and the Yangtze River, which deliver different aged OC (Wang et al., 2012; Wu et al., 2013; Tao et al., 2016). Several prior studies have evaluated the burial efficiency of fluvially delivered OC_{terr} in eastern China marginal sea surface sediments. The $\delta^{13}C$-based OC loading approach revealed lower OC_{terr} burial efficiency in the East China Sea (ECS) inner shelf (25 ± 5%) than proximal to the Yellow River (71 ± 16%, $n = 7$) (Wu et al., 2013; Hou et al., 2020). High burial efficiencies adjacent to the Yellow River and along its transport pathway in Bohai Sea and Yellow Sea (BS-YS) sediments were also supported by terrestrial biomolecular loading approach (Hou et al., 2020). Very high burial efficiencies in the BS-YS for non-modern OC_{terr} (close to 100% for pre-aged OC and 70% for fossil OC) were estimated using mass-balance budgets based on limited available biomarker ^{14}C data (Tao et al., 2016). However, a lack of spatially-resolved information of OC_{terr} burial hinders the elucidation of underlying mechanisms that influence the fate of OC_{terr}, assessment of changes along sediment transport and dispersal pathways, and development of pan-marginal sea carbon budgets.

In this study, we measured the contents and carbon isotopes ($\delta^{13}C$ and $\Delta^{14}C$) of total OC (TOC), mineral SA, and grain size of a suite of surface (~0–5 cm) sediment samples

($n = 98$) from the BS-YS system, and determined lipid biomarker (*n*-fatty acids, *n*-FAs) $\delta^{13}C$ and $\Delta^{14}C$ values for a sub-set of 11 samples. These data were combined with previously published results (Bao et al. 2018b; Tao et al. 2016; Fig. 1) in order to (1) derive spatially-resolved distribution of proportions and contents for specific OC_{terr} pools in the BS-YS system; (2) examine the magnitude and potential causes of changes in loadings of different OC pools from the Yellow River to marine sediments; and (3) highlight novel constraints on the burial potential of different OC_{terr} pools. In most prior studies, assessments of burial efficiency have been based on OC_{terr} residing in the surface mixed layer (upper few centimeters) of continental margin sediments, which does not constitute long-term burial *sensu stricto*. Here, we adopt the terms "burial potential" or "proto-burial" in order to highlight that our findings refer to the earliest stages of burial.

2. MATERIALS AND METHODS

2.1. Study area and sampling

The BS-YS comprises a part of the expansive, shallow (max. depth, 140 m) and semi-enclosed eastern China marginal sea system (Fig. 1). The BS has an area of 77,000 km^2 with an average water depth of 18 m. It is surrounded by the Liaodong and Shandong peninsulas and connected to the northern YS by the Bohai Strait. The YS covers an area of about 400,000 km^2, with an average water depth of 44 m. High sediment accumulation rates near the modern Yellow River estuary (3–7 g cm^{-2} yr^{-1}) and a decreasing seaward trend reflect the direct impact of Yellow River discharge to the BS (Hu et al., 2016). A significant fraction of the exported sediment is subsequently resuspended, transported and re-deposited, resulting in several mud depocenters in Bohai Bay, along the coastal Shandong Peninsula, and in the central BS and YS (Qiao et al., 2017). The average sediment OC burial flux and sequestration on a 100-year timescale has been estimated at 15.3 g m^{-2} yr^{-1} and 5.6 Mt yr^{-1}, respectively (Hu et al., 2016). The Yellow River discharged into the YS from 1128 to 1855 CE, but has discharging into the BS at its current location since 1855 CE (Fig. 1). Nevertheless, erosion from the abandoned old Yellow River delta has remained an important sediment source to the YS and the ECS, contributing >790 Mt yr^{-1} sediment on average for the last 100 years (Zhou et al., 2014).

Ninety-seven surface sediment samples (0–5 cm) covering the BS-YS were collected using a box core sampler during an open cruise supported by the National Natural

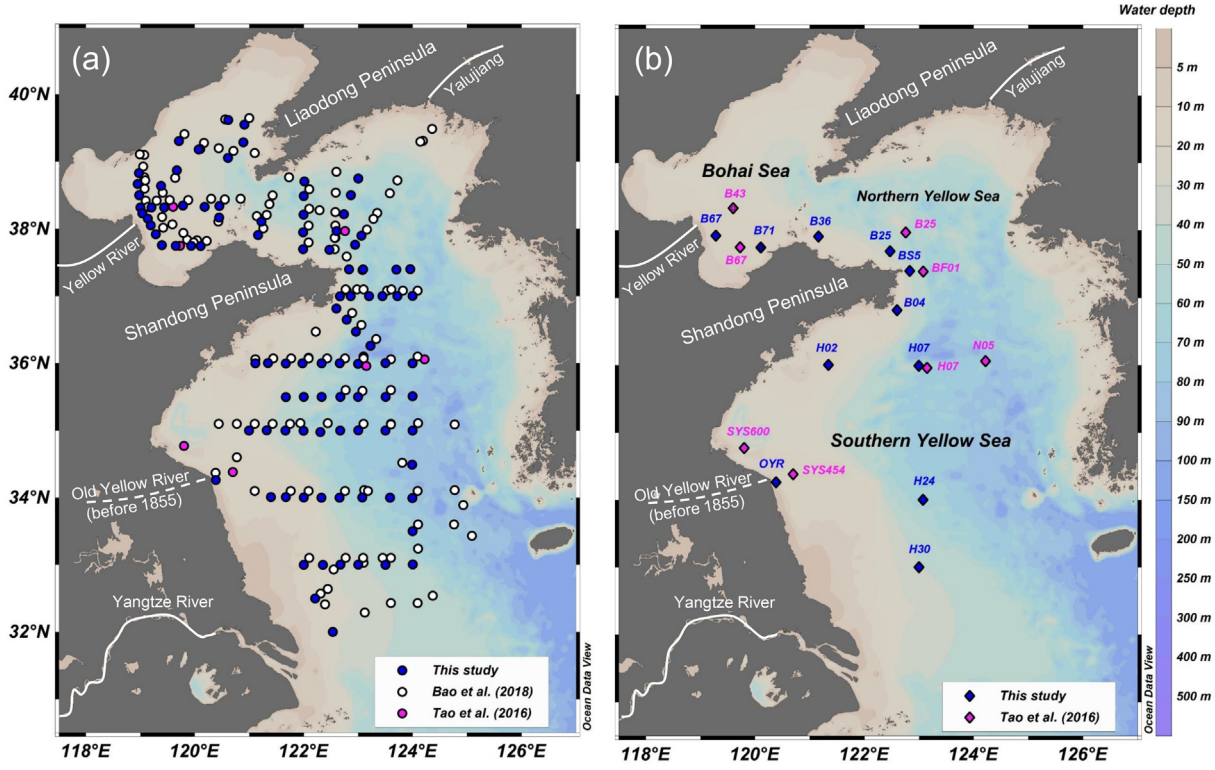

Fig. 1. (a) Locations of sampling sites ($n = 234$) in the Bohai Sea and Yellow Sea (BS-YS) for bulk parameter analyses. Filled blue dots represent surface sediments analyzed in this study ($n = 98$); white ($n = 128$) and pink ($n = 8$) dots represent published data from Bao et al. (2018b) and Tao et al. (2016), respectively. (b) Blue diamonds represent samples ($n = 11$) from this study for compound-specific carbon isotopic ($\delta^{13}C$ and $\Delta^{14}C$) analysis. Pink diamonds ($n = 8$) represent samples with published compound-specific carbon isotopic ($\delta^{13}C$ and $\Delta^{14}C$) data from Tao et al. (2016). For clarity, sample coordinates from Bao et al. (2018b) and Tao et al. (2016) are slightly displaced to avoid overlap (Fig. S1). The map was generated by Ocean Data View software (Schlitzer, 2018). (For interpretation of the references to colour in this figure legend, the reader is referred to the web version of this article.)

Science Foundation of China (*R/V Dongfanghong II*, Ocean University of China) in August of 2015 (Fig. 1). In addition, a subsurface sediment (OYR, 5–10 cm) sample was collected from the Old Yellow River delta in April 2014. All samples were stored at −20 °C and subsequently freeze-dried prior to laboratory analyses. Elemental and bulk carbon isotopic analyses were performed on all samples, while molecular carbon isotope analyses were carried out on eleven samples mostly along the main sediment dispersal pathway (Fig. 1).

2.2. Bulk analysis

After decarbonation by fumigation with 12 N HCl (60 °C, 72 h) (Komada et al., 2008) and subsequent neutralization over NaOH pellets (60 °C, 72 h), the TOC content (TOC%), and carbon isotope composition ($\delta^{13}C$ and $\Delta^{14}C$ values) of TOC was determined using an elemental analyzer (EA, vario MICRO cube, Elementar) coupled to an isotope ratio mass spectrometer (IRMS, Vision, Isoprime) and a gas-ion source Mini Carbon Dating System (MICADAS), respectively, at the Laboratory for Ion Beam Physics, ETH Zürich (McIntyre et al., 2017). After removal of organic matter at 350 °C for 12 h, another aliquot of sediment sample was measured for mineral-specific SA using a 5-point Brunauer-Emmett-Teller (BET) method by NOVA 4000 surface area analyzer, and for grain size distribution by Malvern Mastersizer 2000.

2.3. Biomarker extractions and compound-specific carbon isotope analysis

Methods for extraction, purification and isolation of target compounds (*n*-FAs) have been previously reported (Tao et al., 2015; Yu et al., 2019a). Stable carbon isotopic compositions ($\delta^{13}C$ values) of target compounds were determined by gas chromatograph-isotope ratio mass spectrometry (GC-IRMS) and were measured in in duplicate. Corresponding ^{14}C contents ($\Delta^{14}C$ values) were determined using a gas-ion source MICADAS system at ETH Zürich (Christl et al., 2013). Detailed descriptions of the experimental methods are provided in the Supplementary materials (Text S1). C_{16FA}, C_{18FA}, C_{24FA} and $C_{26+28+30FAs}$ were generally collected for $\Delta^{14}C$ analysis. The $C_{26+28+30FAs}$ were combined because individual FA amounts were insufficient for $\Delta^{14}C$ analysis.

2.4. Dual carbon isotope mixing model

Since bulk $\delta^{13}C$ and $\Delta^{14}C$ values are generally insufficient to distinguish the pre-aged (soil) OC from modern/-contemporary OC and fossil OC because of overlapping endmember isotopic compositions, a dual carbon isotope mixing model based on both bulk and molecular $\delta^{13}C$ and $\Delta^{14}C$ values is used to constrain proportions of the three OC pools, i.e., OC_{modern}, $OC_{pre\text{-}aged}$, and OC_{fossil} pools (Drenzek et al., 2007; Tao et al., 2016). The relative fractional contribution of OC_{modern} (f_{modern}), $OC_{pre\text{-}aged}$ ($f_{pre\text{-}aged}$), OC_{fossil} (f_{fossil}) pools to sedimentary TOC is estimated by the following equations:

$$\Delta^{14}C_{TOC} = f_{modern} \times \Delta^{14}C_{modern} + f_{pre-aged} \times \Delta^{14}C_{pre-aged} + f_{fossil} \times \Delta^{14}C_{fossil} \quad (1)$$

$$\delta^{13}C_{TOC} = f_{modern} \times \delta^{13}C_{modern} + f_{pre-aged} \times \delta^{13}C_{pre-aged} + f_{fossil} \times \delta^{13}C_{fossil} \quad (2)$$

$$1 = f_{modern} + f_{pre-aged} + f_{fossil} \quad (3)$$

where $\delta^{13}C_{TOC}$ and $\Delta^{14}C_{TOC}$ are the measured values of sediment samples. The $\delta^{13}C$ and $\Delta^{14}C$ values of OC_{modern}, $OC_{pre\text{-}aged}$ and OC_{fossil} are constrained by carbon isotopic compositions of specific endmember biomarkers (see Section 4.1 and Supplementary Text S2). Although biomarkers generally comprise only a small portion of bulk OC, they retain the isotopic signals of the corresponding carbon sources and avoid interference from other carbon pools (Eglinton et al., 1997). After accounting for offsets in $\delta^{13}C$ between source-specific biomarker and bulk biomass ($\delta^{13}C_{bulk} - \delta^{13}C_{lipid}$) resulting from biosynthetic fractionation and related effects (e.g., Collister et al., 1994; Schouten et al., 1998), the isotopic signatures of biomarkers are used to solve a set of simultaneous isotopic mass balance expressions to yield the fractional abundances of the OC sources they represent. We applied an offset of 4-7‰ to measured biomarker $\delta^{13}C$ values, as previously applied in the BS-YS OC source apportionment study (Tao et al., 2016 and references therein). With limited data, previous studies uniformly applied the measured compound-specific carbon isotopic values in each sample to define endmembers. In this study, we utilize $\delta^{13}C$ and $\Delta^{14}C$ data of *n*-FAs from 18 sites (with exception of N05, see Text S2) that encompass a large swath of the BS-YS region (Fig. 1b). Mean values with the standard deviation were used to constrain endmember isotopic values, in order to account for variability and uncertainties (e.g., Vonk et al., 2010; Lin et al., 2019). The dual carbon isotope mixing model was then applied to all bulk samples (Fig. 1a) in order to assess spatial variability among OC pools of different age. To test the robustness of endmember assignment, we compared results from different endmember source assignments and data size, and found no significant differences in the distribution patterns and in the arithmetic mean values in surface sediments (see details in Text S3). A Bayesian Markov chain Monte Carlo (MCMC) simulation was applied to minimize errors from arbitrary assignments of endmember values (Andersson et al., 2015; Yu et al., 2019a). Briefly, 1,000,000 out of 100,000,000 random samples from the normal distribution of each endmember within the given mean and standard deviation were taken to simultaneously fulfill the given system (Eqs. (1)–(3)) in simulations. The mean relative contributions and the standard deviation of different aged OC pools were then estimated.

3. RESULTS

3.1. Bulk sedimentary characteristics

In this study, we report a new data set ($n = 98$) of TOC %, SA, mean grain size, OC/SA ratio, TOC $\delta^{13}C$ and $\Delta^{14}C$ values of BS-YS surface sediments (Table S1). There were

no significant differences in bulk properties ($p > 0.05$) between this study and prior studies ($n = 136$, Bao et al. 2018b; Tao et al. 2016). One exception is the mean $\delta^{13}C$ value, which is slightly higher ($-21.9 \pm 0.5‰$, mean ± S.D.) than from previous studies ($-22.1 \pm 0.6‰$). In addition, spatial variations of bulk properties in this study (Fig. S2) are consistent with those reported in Bao et al. (2018b). Thus, all data were combined to examine spatial variations in bulk properties (Fig. 2).

TOC contents (TOC%) ranged from 0.04% to 1.37%, with a mean of 0.51 ± 0.30% ($n = 233$). Higher TOC% values were observed in western BS and the northern-central YS (Fig. 2a), mostly in fine-grained mud areas (Fig. 2c), as reflected by the relationship between TOC% and mean grain size (Fig. S3a). Lower TOC% values were mostly found in the Bohai strait and along the YS coast, with the lowest values in the sand area of the northeastern part of northern YS. SA values ranged from 2.0 to 40.3 $m^2\ g^{-1}$ (ave., 16.5 ± 8.8 $m^2\ g^{-1}$, $n = 225$), with similar spatial distribution to that of TOC% and fine-grained mud (Fig. 2b and 2c), reflecting the larger SA of finer particles (Fig. S3b). Mean grain size varied from 6.3 to 448.7 μm (ave., 52.5 ± 62.3 μm, $n = 230$), with lower values representing the clayey silt and silt sediments (i.e., fine-grained mud deposits, Fig. 2c) (Qiao et al., 2017). TOC/SA ratios (i.e., TOC loadings) ranged from 0.09 to 0.73 mg C m^{-2} (ave., 0.31 ± 0.10 mg C m^{-2}, $n = 224$), with highest values near the eastern coast of Liaodong Peninsula and lowest values near the Old Yellow River delta (Fig. 2d).

The $\delta^{13}C_{TOC}$ values ranged from −19.9 to −25.9‰, with an average value of $-22.0 \pm 0.6‰$ ($n = 234$). Lower values mainly occurred near the modern and Old Yellow River delta, while higher values were mostly observed in the southern YS (Fig. 2e). $\Delta^{14}C_{TOC}$ values ranged from −137 to −678‰ (corresponding to conventional ^{14}C ages of 1125–9036 yr) with an average value of $-269 \pm 78‰$ (2461 ± 855 ^{14}C yr; $n = 234$). Higher values were broadly distributed in the BS and YS basins (much higher values in the fine-grained area of northern YS), while lower values were found near river deltas, especially near the Old Yellow River delta (Fig. 2f).

3.2. *n*-Fatty acid contents and carbon isotopic compositions

Straight-chain fatty acids (*n*-FAs) in BS-YS sediments exhibited a bimodal distribution with an even-carbon num-

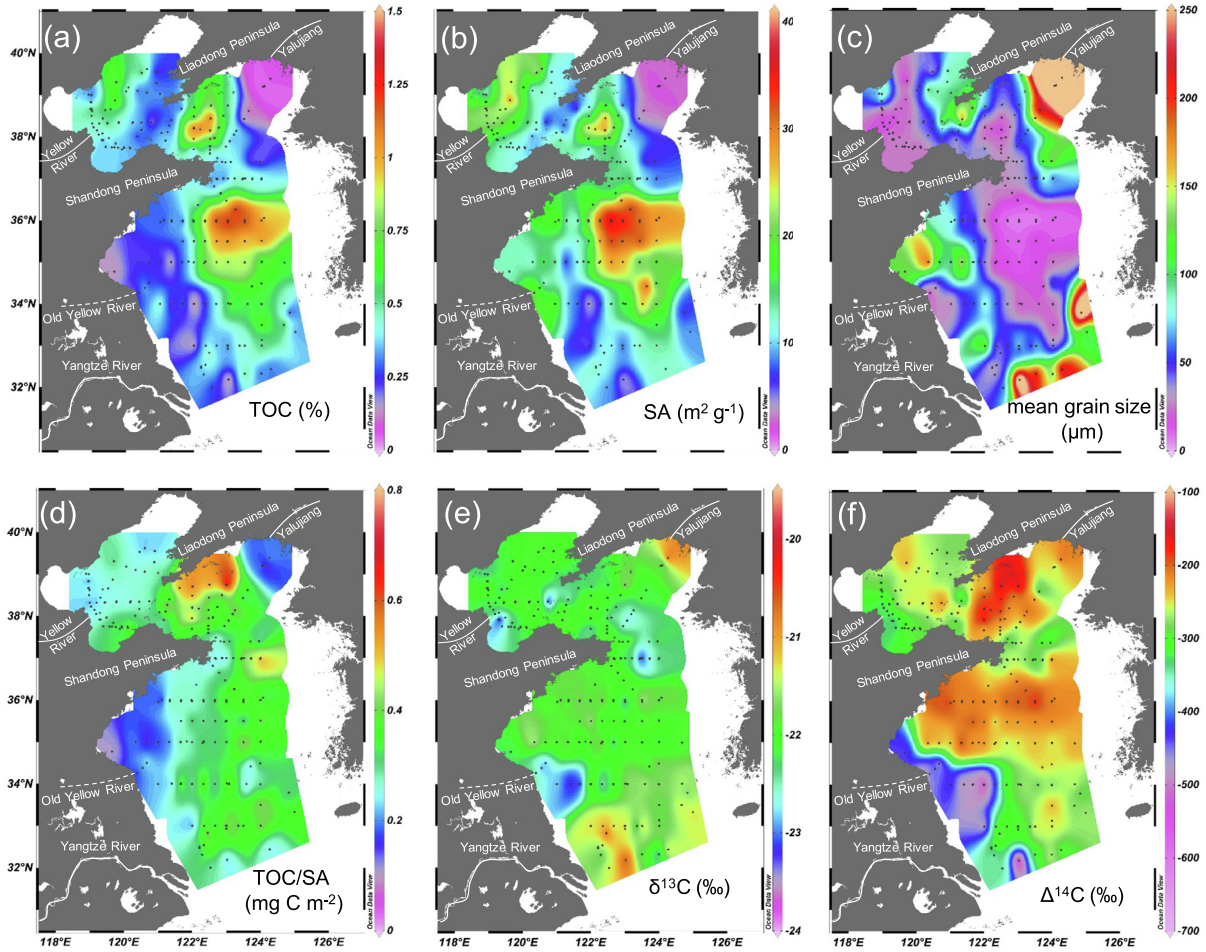

Fig. 2. Spatial variations of (a) TOC (%, $n = 234$); (b) SA ($m^2\ g^{-1}$, $n = 225$); (c) mean grain size (μm, $n = 230$); (d) TOC/SA ratios (mg C m^{-2}, $n = 224$); (e) $\delta^{13}C$ (‰, $n = 234$) and (f) $\Delta^{14}C$ (‰, $n = 234$) in surface sediments from the BS-YS. New datasets ($n = 98$) are from this study (Table S1), with others from Bao et al. (2018b) and Tao et al. (2016).

ber predominance in the range of C_{14-32}, with C_{max} at C_{16} among the short-chain homologues, and C_{24}/C_{26} in the long-chain counterparts (Fig. S4, Table S2). The carbon preference index for long-chain *n*-FAs ($CPI_{\Sigma 24-32FA}$) ranged from 4.1 to 5.6 (ave., 4.6 ± 0.5, $n = 11$). TOC-normalized contents of C_{16FA}, C_{18FA}, C_{24FA}, long-chain $C_{26+28+30FAs}$ and total *n*-FAs (μg g^{-1} OC) ranged from 193 to 1268, 61 to 177, 47 to 189, 90 to 358 and 593 to 2803, respectively. The highest TOC-normalized content of $C_{26+28+30FAs}$ was found in Yellow River estuary (B67), and exhibited a decreasing trend along the sediment transport pathway around the Shandong peninsula, with the lowest contents observed at sites H07 and OYR. Short-chain *n*-FA contents did not exhibit a clear spatial pattern, with the highest values at sites B25 and B67 but the lowest values at sites H07 and OYR.

Sediments selected for *n*-FA $\delta^{13}C$ and $\Delta^{14}C$ analyses in this study ($n = 11$) were mainly located along the Yellow River sediment transport pathway (Table S2). Combined with previously reported data ($n = 8$) from Tao et al. (2016), these afforded spatial coverage over the BS-YS ($n = 19$) in *n*-FA $\delta^{13}C$ and $\Delta^{14}C$ values.

The $\delta^{13}C_{FAs}$ values in this study ranged from −22.4 to −30.9‰, with higher values for short-chain *n*-FAs (C_{16}, C_{18}) (−22.4 to −29.1‰) than longer-chain homologues (C_{24}, $C_{26+28+30FAs}$) (−25.8 to −30.9‰). $\delta^{13}C_{16FA}$ and $\delta^{13}C_{18FA}$ values showed larger ranges and were on average 0.7–1.5‰ higher than published data, while $\delta^{13}C_{24FA}$ and $\delta^{13}C_{26+28+30FAs}$ fell in the similar range to published results (Fig. 3). The highest short-chain $\delta^{13}C_{FA}$ values from this study were found at site H30, while the lowest values were found at site OYR (Figs. S5a and b). For longer-chain homologues, the lowest $\delta^{13}C$ values were observed at modern and old Yellow River deltas (B67 and OYR, Figs. S5c and d), which showed similar pattern to those from Tao et al. (2016).

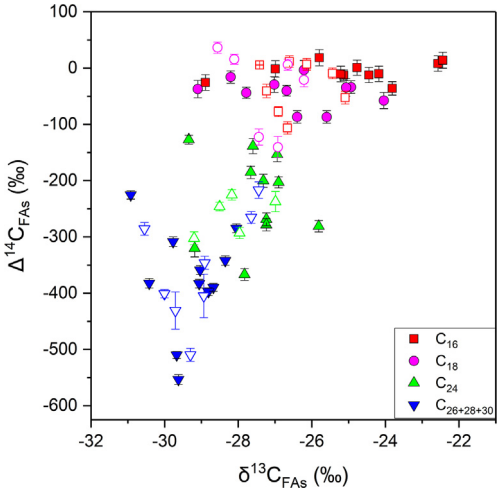

Fig. 3. Cross plot of $\delta^{13}C$ versus $\Delta^{14}C$ values of *n*-FAs in surface sediments from the BS-YS. Filled symbols represent samples in this study ($n = 11$) and open symbols are for published results ($n = 8$) from Tao et al. (2016). Different symbol types and colors correspond to different FA chain lengths. (For interpretation of the references to colour in this figure legend, the reader is referred to the web version of this article.)

$\Delta^{14}C_{FAs}$ values in this study exhibited significant variability, ranging from +19 ± 14 to −553 ± 9‰ (^{14}C ages from modern to 6410 yr), a similar range to published results (Fig. 3). Short-chain C_{16FA} and C_{18FA} (+19 ± 14 to −36 ± 12‰, −3 ± 17 to −87 ± 11‰, respectively) tend to be more ^{14}C-enriched than longer-chain C_{24FA} and $C_{26+28+30FAs}$ (−127 ± 8 to −367 ± 11‰, −226 ± 7 to −553 ± 9‰, respectively). The highest $\Delta^{14}C_{26+28+30FAs}$ value was found in modern Yellow River delta (site B67) while the lowest value was found at site H30 (Fig. S6).

All $\delta^{13}C$ and $\Delta^{14}C$ values of *n*-FAs in BS-YS sediments ($n = 19$) revealed two clear patterns (Fig. 3). First, both $\delta^{13}C_{FAs}$ and $\Delta^{14}C_{FAs}$ values exhibited a decreasing trend with increasing chain length. Second, C_{16FA} and C_{18FA} exhibited a larger range of $\delta^{13}C$ values (−22.4 to −28.9‰, −24.0 to −29.1‰, respectively) but a narrower range of $\Delta^{14}C$ values (+19 ± 14 to −106 ± 11‰, +37 ± 10 to −140 ± 19‰, respectively) than C_{24FA} and $C_{26+28+30FAs}$. The latter showed a larger range of $\Delta^{14}C$ values (−127 ± 8 to −367 ± 11‰, −217 ± 15 to −553 ± 9‰, respectively) but a narrower range of $\delta^{13}C$ values (−25.8 to −29.3‰, −27.4 to −30.9‰, respectively).

4. DISCUSSION

In the following sections, we first discuss OC heterogeneity and constrain different OC pools, i.e., OC_{terr} based on a conventional $\delta^{13}C_{TOC}$ source apportionment approach, as well as OC_{modern}, $OC_{pre\text{-}aged}$, and OC_{fossil} based on an approach established by Tao et al. (2016), focusing on spatial variations among different OC pools. Using the relationship between contents of different OC pools and mineral SA, we examine the changes of loadings from river to sediments, leading to preliminary discussion on mechanisms responsible for the burial potential and fates of different terrestrial OC pools in the BS-YS.

4.1. Characteristics and spatial heterogeneity of sedimentary OC

Radiocarbon ages (1125 and 9036 ^{14}C yr) of surface-sediment OC were significantly older than depositional ages (<100 yr, estimated from ^{210}Pb measurements, Hu et al., 2016) in the BS-YS, implying an important contribution of pre-aged OC and fossil OC (Fig. 4a). Our new maps of biomarker $\delta^{13}C$ and $\Delta^{14}C$ values facilitate definition of specific OC source endmembers (Fig. 4b), which in turn allow assessment of spatially-resolved contributions to bulk samples using dual carbon isotope mixing model (Section 2.4). Molecular $\delta^{13}C$ and $\Delta^{14}C$ constraints on the OC provenance are described in Supplementary Text S2. In summary, we assign mean values (with the standard deviation; $n = 18$, with exception of N05, see Text S2) of all measured $\delta^{13}C$ and $\Delta^{14}C$ values of *n*-C_{16FA} as modern OC endmember (mixture of fresh marine and/or terrestrial OC), and of *n*-$C_{26+28+30FAs}$ as pre-aged OC_{terr} endmember, as well as previously published even-carbon number $C_{16-+18Alkanes}$ values as fossil OC endmembers (mainly originating from ancient bedrock erosion, Tao et al., 2016; Sun et al., 2018). These endmembers are well separated from

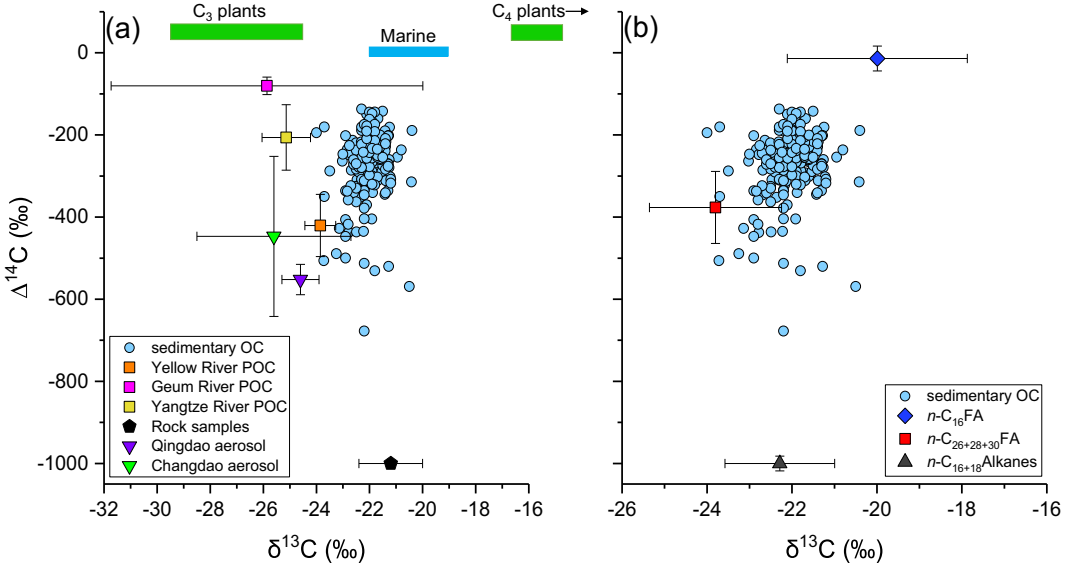

Fig. 4. Scatter plots of $\delta^{13}C$ versus $\Delta^{14}C$ values of surface-sediment OC (filled circles) and plausible endmembers (filled symbols). (a) Possible sources of OC including typical C_3 and C_4 plants from Chinese Loess Plateau (Liu et al., 2003), marine phytoplankton (Fry and Sherr, 1984), Yellow River POC (Wang et al., 2012; Xue et al., 2017; Tao et al., 2018; Yu et al., 2019a), Geum River POC (Kang et al., 2020), Yangtze River POC (Wang et al., 2012; Wu et al., 2018), and rock samples from the western Chinese Loess Plateau (Liu et al., 2007), as well as aerosols from coastal city (Qingdao and Changdao) in Shandong peninsula (Yu et al., 2018a). $\Delta^{14}C$ values of modern sources and ancient rocks are assigned as 0 ± 50‰ and –1000‰ respectively (Goñi et al., 2005). (b) The $\delta^{13}C$ and $\Delta^{14}C$ values of source-specific biomarkers (n-C_{16FA}, n-$C_{26+28+30FAs}$ and n-$C_{16+18Alkanes}$) are shown as filled diamond, square and triangle symbols, where $\delta^{13}C_{FAs}$ were corrected by 4–7‰ in order to compensate for $\delta^{13}C_{bulk} - \delta^{13}C_{lipid}$ fractionation (Tao et al., 2016 and references therein).

each other (Fig. 4b). To derive spatially-resolved distributions of different aged OC pools, the dual carbon isotopic mixing model (Eqs. (1)–(3)) was applied to all bulk samples and all possible solutions derived from MC simulations are shown in Fig. 5 and Table S3. For comparison, a fractional contribution of OC_{terr} (%) was also estimated using a conventional $\delta^{13}C_{TOC}$ approach based on a binary mixing model that has been widely used to estimate the proportions of terrestrial and marine OC sources in the BS-YS sediments and other marginal sea sediments (e.g., Burdige, 2005; Lamb et al., 2006; Belicka and Harvey, 2009; Xing et al., 2014; Liu et al., 2015; Yoon et al., 2016). Given the dominant influence of Yellow River, the terrestrial endmember $\delta^{13}C$ value was obtained from measured $\delta^{13}C$ values of Yellow River particulate OC (POC), which is −23.9 ± 0.6‰ (n = 34, Wang et al., 2012; Xue et al., 2017; Tao et al., 2018; Yu et al., 2019a). OC produced by marine organisms typically exhibits $\delta^{13}C$ values between −19‰ and −22‰, thus, a global average value of −20‰ is widely used as marine OC endmember (Fry and Sherr, 1984; Goñi et al., 2005) when lacking of specific values for the study areas. In our study area, a $\delta^{13}C$ value of −20.3 ± 1.3‰ has been used as marine endmember based on phytoplankton OC data in BS (Liu et al., 2015), and −20 ± 1.0‰ has previously been used as marine endmember in YS (Xing et al., 2014; Xing et al., 2016; Yoon et al., 2016). Thus, for consistency with other studies, $\delta^{13}C$ values of −20.3‰ and −20‰ are assigned as the marine OC endmember for BS and YS, respectively, in the binary mixing model. Broad-scale, spatial patterns of fractional contributions and contents of OC_{modern}, $OC_{pre\text{-}aged}$ and OC_{fossil}, as well as OC_{terr} in BS-YS sediments were then obtained (Fig. 5, Fig. S7 and Table S3).

Fractional contributions (%) of the three different aged OC pools (modern, pre-aged, fossil) exhibited different ranges and spatial variabilities in the BS-YS sample suite (n = 232; Fig. 5a–c). OC_{modern} is a dominant component of sedimentary OC, accounting on average for 49 ± 10% of TOC (17–71%). Higher OC_{modern}% values mainly occurred in BS basin and northern-central YS, while lower values are mainly observed near the Old Yellow River and modern Yellow River delta (Fig. 5a). $OC_{pre\text{-}aged}$ ranged from 19% to 59% (ave., 37 ± 6%), with higher values near modern and old Yellow River delta (Fig. 5b). OC_{fossil} accounts for 13 ± 6% (6–57%) of TOC and exhibited distinct distribution with higher values mainly occurring in coastal area along Old Yellow River delta and in proximity to the modern Yellow River delta, while lower values mostly occurred in the basin areas (Fig. 5c). The similar spatial distributions of $OC_{pre\text{-}aged}$ and OC_{fossil} underline the influence of fluvial input and the terrestrial origin of these OC pools. These two pools contribute an average of 51 ± 10% (29–83%) to sedimentary OC, which was broadly equal to that estimated for OC_{terr} % by the bulk OC $\delta^{13}C$ approach (10–97%, ave., 51 ± 14%, n = 231, Fig. S7). OC_{terr}% shows similar spatial distribution pattern to that of $OC_{pre\text{-}aged+fossil}$%, both with higher values near river delta areas (Fig. S7). This clearly suggests that OC_{terr} in BS-YS sediments is mainly composed of millennial-aged and fossil OC, with the former being predominant. Thus,

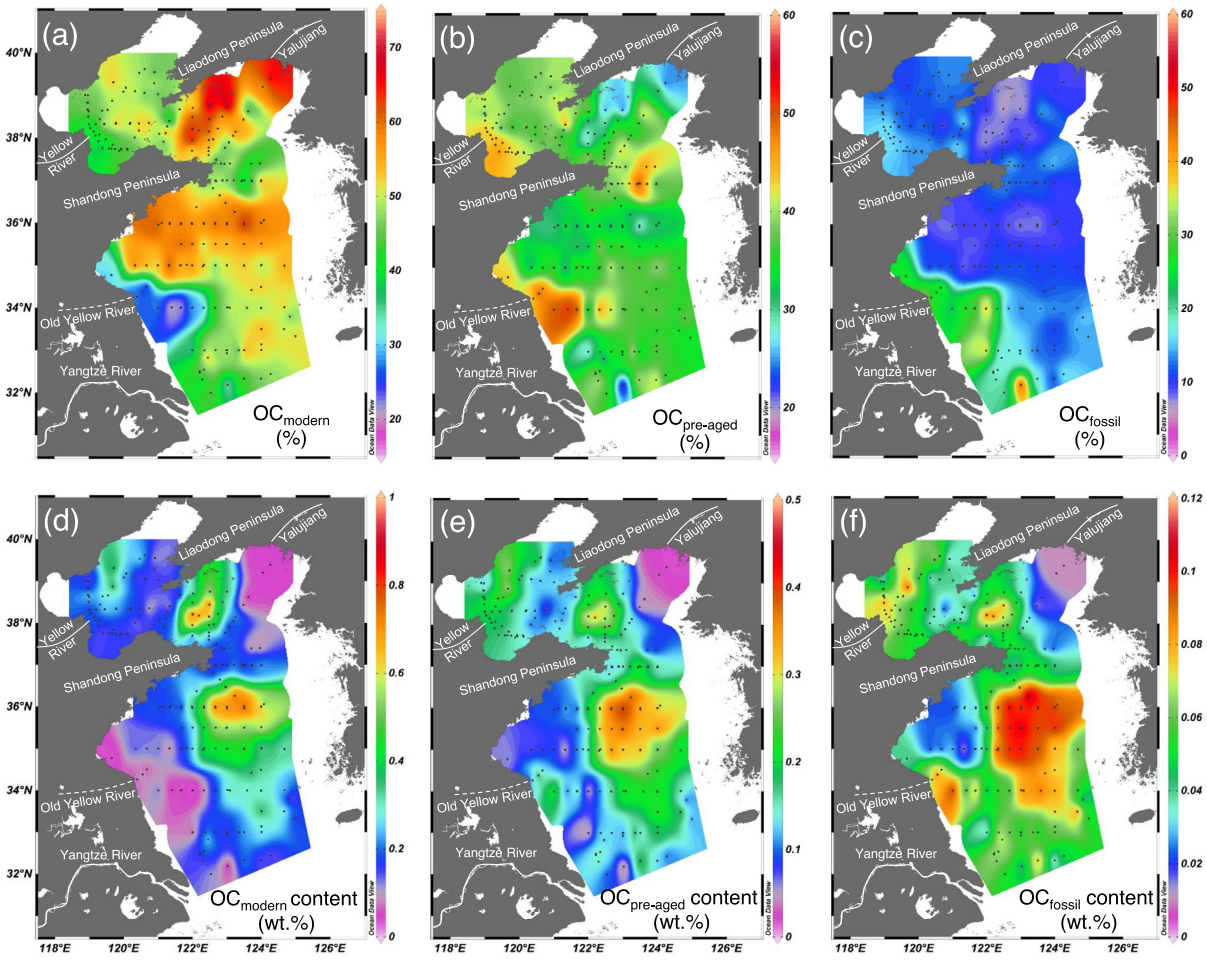

Fig. 5. Spatial variations of fractional abundance (%, a–c) and contents (wt.%, d–f) of different OC pools.

the ^{14}C age of OC source is an important contributor to the non-modern sedimentary OC ^{14}C ages of BS-YS surface sediments.

Contents of different OC pools were obtained by multiplying TOC content by fractional abundance of the corresponding OC pools. Thus, contents (wt.%) of OC_{modern}, $OC_{pre\text{-}aged}$, OC_{fossil} and OC_{terr} ranged from 0.01 to 0.96 (ave., 0.27 ± 0.19), from 0.01 to 0.49 (ave., 0.18 ± 0.09), from 0.01 to 0.12 (ave., 0.06 ± 0.03), and from 0.01 to 1.30 (ave., 0.26 ± 0.17), respectively. The contents of OC_{terr} and different aged OC pools show different spatial patterns from their corresponding fractional contributions, but they all show broadly similar patterns to those of TOC% and SA, with higher values in the BS basin and mud areas of northern and central YS (Fig. 5d–f and Fig. S7). This implies the distal mud areas represent important depocenters for fine-grained sediments and associated OC (Hu et al., 2011; Hu et al., 2016). OC_{modern} contents showed increasing trend from the coast to the basin, which is consistent with the distribution of marine phytoplankton biomarkers (Xing et al., 2011; Yu et al., 2018b), and implies that OC_{modern} is dominated by marine OC. Higher contents of $OC_{pre\text{-}aged}$ and OC_{fossil} are observed in coastal areas, especially near the modern and Old Yellow River deltas, reflecting their terrestrial (fluvial) source.

4.2. Loadings of different OC pools

Previous studies have shown that mineral protection is an important controlling mechanism that regulates long-term preservation of OC in marine sediments (Keil et al., 1994; Mayer, 1994a, b), with the degree of OC stabilization during transport and sedimentation depending on both organic matter and mineral type (Blattmann et al., 2019; Hemingway et al., 2019). Generally, higher TOC% values are coincident with higher mineral SA values, as found in fine-grained mud areas in this study (Fig. 2). Superior preservation of OC associated with fine particles is further supported by the strong positive relationships among SA, mean grain size and TOC% (Fig. 6a and S3). Sedimentary OC in the BS-YS was largely, although not exclusively, associated with mineral surfaces ($R^2 = 0.72$, $p < 0.01$, Fig. 6a). Normalizing OC concentrations to mineral-specific SA helps to account for the effects of both physical sorting and mineral association on spatial variations in TOC, given that SA is linked to both aspects (Blair and Aller, 2012). Most of the TOC loadings (ave., 0.31 ± 0.10 mg C m^{-2}, $n = 224$) in the BS-YS sediments fell below the range of typical riverine and shelf sediments (0.4–1.0 mg C m^{-2}, Fig. 6a, Blair and Aller, 2012), and are lower than sediments in the ECS and northern South China Sea

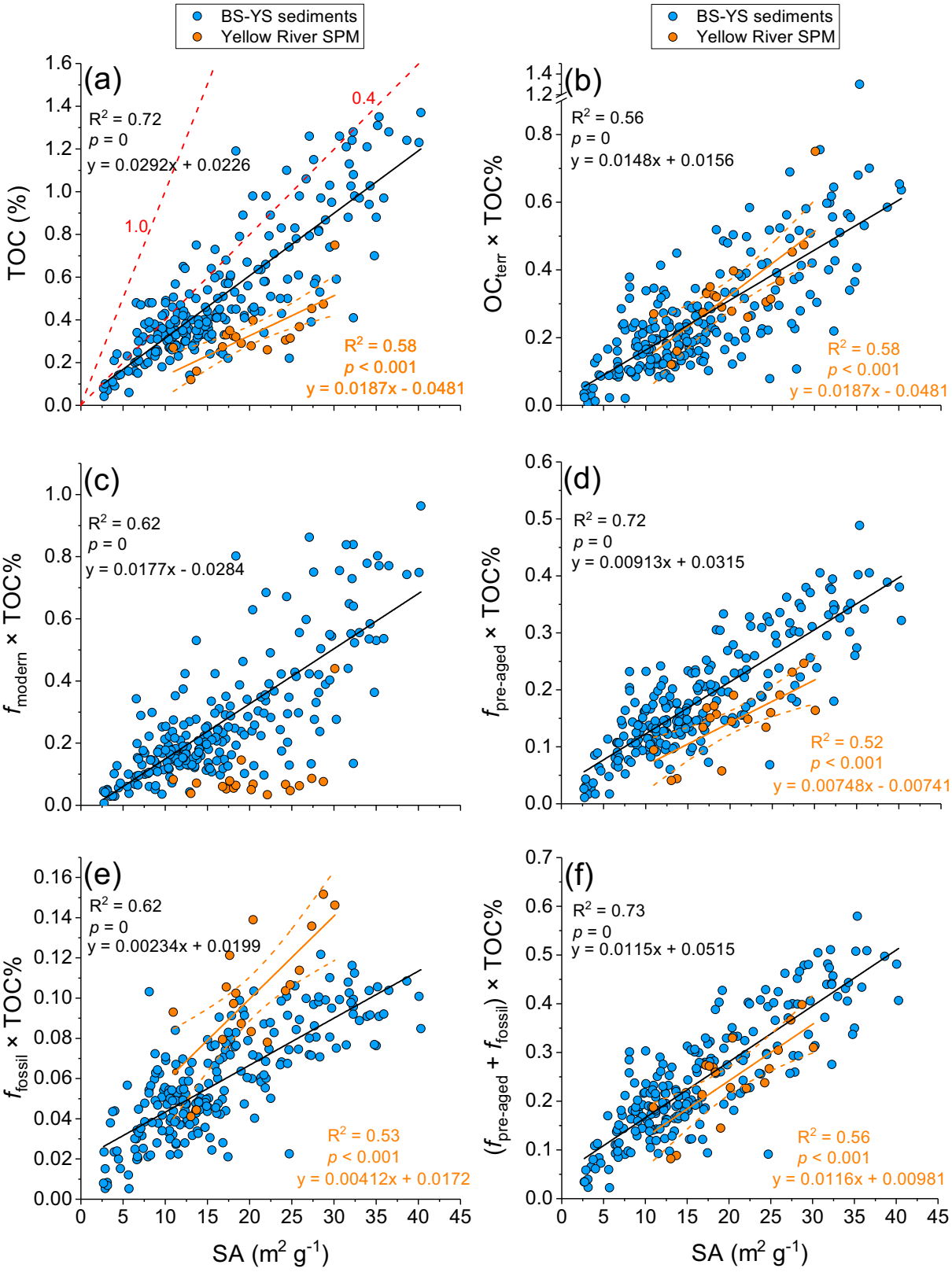

Fig. 6. Plots of SA ($m^2\ g^{-1}$) versus (a) TOC content (%); (b) OC_{terr} content (%); (c) OC_{modern} content (%); (d) $OC_{pre\text{-}aged}$ content (%); (e) OC_{fossil} content (%) and sum content of $OC_{pre\text{-}aged}$ and OC_{fossil} (%) in the BS-YS surface sediment samples (blue) and Yellow River SPM samples (orange). Dashed red lines in panel (a) represent the TOC/SA ratios between 0.4 and 1.0 mg C m^{-2} (Blair and Aller, 2012). Dashed lines for Yellow River SPM samples represent the 95% confidence interval of regression line. (For interpretation of the references to colour in this figure legend, the reader is referred to the web version of this article.)

(SCS) (Bao et al., 2018b; Hou et al., 2020), but higher than that of lower Yellow River suspended particulate matter (SPM, Fig. 6a, 0.16 ± 0.04 mg C m^{-2}, $n = 18$, Tao et al., 2015; Yu et al., 2019a). The increases of TOC loading and $\delta^{13}C$ values from riverine SPM to marine sediments suggests addition of and/or replacement by marine OC (Keil et al., 1997; Blair and Aller, 2012).

Similar to TOC loadings, normalizing different OC pools to SA facilitates comparison of net changes of different OC pools, as previously used to trace the fate of terrestrial OC during riverine and cross-shelf transport (Keil et al., 1997; Goñi et al., 2005; Aller et al., 2008; Tesi et al., 2014; Bröder et al., 2016; Bröder et al., 2018; Freymond et al., 2018). The contents of OC_{terr} and different aged OC pools in our BS-YS samples all exhibit strong association with mineral surfaces (R^2 values range from 0.56 to 0.72, $p < 0.01$, Fig. 6b–e), with the tightest coupling for $OC_{pre\text{-}aged}$ content. This suggests an important role of mineral surfaces on potential OC_{terr} burial in BS-YS. Both sediment mass balance and sediment source studies have shown that the BS-YS system is dominantly influenced by the Yellow River (Yang et al., 2003; Qiao et al., 2017 and references therein). Given that suspended material exported by this fluvial system is mainly eroded from the Loess Plateau, modern and Old Yellow River mineralogy should be similar. The $\delta^{13}C$ and $\Delta^{14}C$ values of sedimentary OC in BS-YS also support the predominant influence of the Yellow River (Fig. 4a). On the other hand, rivers discharging from the western coast of Korea into Yellow Sea may have influences on the eastern Yellow Sea proximal to the Korean Peninsula, but the sharply contrasting $\delta^{13}C$ and $\Delta^{14}C$ values of POC from Geum River imply limited contributions to northern and central Yellow Sea sediments. This is also the case for Yangtze River (Fig. 4a; Wang et al., 2012; Wu et al., 2018). Thus, given that the BS-YS system is largely influenced by the Yellow River, we compare the relevant parameters against the corresponding relationships for Yellow River SPM samples. OC_{terr} (i.e., fluvial input of POC), $OC_{pre\text{-}aged}$ and OC_{fossil} show significant positive correlation with SA while OC_{modern} does not (Fig. 6a–e). Thus, OC_{modern} in Yellow River SPM likely has different source(s) and associations with mineral particles (Fig. 6c), such as coarse detrital particle matter derived from aquatic and terrestrial (higher plant) productivity (Yu et al., 2019b). In contrast, OC_{modern} in BS-YS sediments is found to be strongly associated with mineral surfaces, although it is likely dominated by marine productivity, especially in the offshore mud areas characterized by high surface area minerals. Strong association of OC_{terr} with minerals was also found in northern SCS sediments (OC_{terr} contents vs. grain size), but not for marine OC (Wei et al., 2020).

OC_{terr} loadings in BS-YS sediments are similar to those of riverine SPM (Fig. 6b). Similar relationships were also found for the Ganges-Brahmaputra-Bengal Fan system (Galy et al., 2007), and suggest efficient accumulation OC_{terr} exported by the Yellow River in BS-YS sediments. Slopes of regression lines (Fig. 6) correspond to average loadings of certain OC pools, revealing higher values for $OC_{pre\text{-}aged}$ but lower values for OC_{fossil} in BS-YS sediments than Yellow River SPM (Fig. 6d and e). This implies different fates of these OC pools during translocation from river to marginal sea sediments, including degradation and aging (Blair and Aller, 2012; Bao et al., 2018a). However, higher overall sedimentary $OC_{pre\text{-}aged}$ loadings than corresponding Yellow River SPM loadings are suggestive of additional sources. Potential candidates are small rivers and/or atmospheric deposition (Matsumoto et al., 2001; Tao et al., 2016; Yu et al., 2018a). In contrast, OC_{fossil} shows decreasing loadings from riverine SPM to marginal sea sediments, implying degradation during transport, different mineral associations (Blattmann et al., 2019), or escape to other (deep) ocean regions (Bao et al., 2019). This molecular isotope-based evidence for the disappearance of OC_{fossil} exported from the Yellow River is supported by other studies (Sun et al., 2018).

Since both $OC_{pre\text{-}aged}$ and OC_{fossil} are of terrestrial origin and are sub-pools of terrestrial OC, we explore the relationship between non-modern OC (i.e., $OC_{pre\text{-}aged} + OC_{fossil}$) contents and SA in order to reduce uncertainties induced from the source apportionment for each OC pool. Besides similar spatial distribution pattern of fractional abundance and contents to those of OC_{terr}, the content of non-modern OC also shows similar relationship versus SA between sediments and riverine SPM. This provides additional evidence that OC_{terr} in BS-YS sediments is dominated by millennial-aged OC which is efficiently preserved (Fig. 6f). The robustness of the regression approach is dependent on the data density and source apportionment results. Uncertainties could arise from the larger dataset for surface sediments ($n = 232$) compared to riverine SPM samples ($n = 18$), and from applying the mean values of biomarker carbon isotopic data as endmembers to all bulk sediment samples. However, changing data size and endmember assignment strategy (measured, including interpolated and fixed mean values) does not significantly change the regression result pattern of different OC pools between sediments and riverine SPM (Supplementary Text S3, Figs. S8–S11). The loading patterns of terrestrial OC pools between riverine SPM and surface sediments based on regression slopes were also consistent with those estimated by arithmetic mean values (Fig. S12). The assigned $\delta^{13}C$ correction to account for $\delta^{13}C_{bulk}$-$\delta^{13}C_{lipid}$ fractionation could also result in larger uncertainties in source apportionment, although MC simulation would account for associated uncertainties. While further ^{14}C approaches, such as coupling with ramped pyrolysis/oxidation (RPO), could place further constraints on different aged OC pools (Hemingway et al., 2019; Hage et al., 2020), the use of molecular carbon isotope-based loadings provides a robust means to evaluate spatial variability in the preservation among OC_{terr} pools.

4.3. The fate of terrestrial OC pools in BS-YS

The changes in loadings of OC_{terr}, $OC_{pre\text{-}aged}$ and OC_{fossil} from the Yellow River to BS-YS sediments, and their spatial distribution patterns in these marginal seas reflect the contrasting fates of these terrestrial OC pools during transport and sedimentation. We here adopt the concept OC loading to evaluate OC_{terr} burial potential (Keil et al., 1997; Burdige, 2005), which is generally estimated by com-

paring values from riverine inputs to marine sediments and most recent studies have mostly focused on surficial sediments (Wu et al., 2013; Vonk et al., 2015; Bröder et al., 2016; Hou et al., 2020; Qi et al., 2021). While OC residing in the upper few centimeters of marine sediments may have not yet passed through the window of early diagenesis, and thus is not buried in the strictest sense, comparisons among terrestrial OC pools by multiple proxies and the corresponding spatially-resolved distributions of surface sediments should presage OC burial.

Although all OC pools exhibit a significant correlation with mineral surface area (Fig. 6), the positive intercepts imply that a certain portion of terrestrially-derived OC is not closely associated with minerals. This could include fragments of plant debris or other low-density particles, including organic-rich aggregates (Wakeham et al., 2009; Tesi et al., 2016; Hage et al., 2020). Thus, the average loadings of OC_{terr}, $OC_{pre\text{-}aged}$ and OC_{fossil} are higher than those derived from regression slopes in Fig. 6. However, they show uniformly high burial potentials, as well as similar proto-burial patterns among different OC_{terr} pools (i.e., similar OC_{terr} loadings, higher $OC_{pre\text{-}aged}$ loadings, lower OC_{fossil} loadings, and higher non-modern OC loadings in BS-YS sediments relative to those of the Yellow River; Fig. S12). This suggests that BS-YS sediments efficiently retain predominantly millennial-aged OC delivered by the Yellow River. This is also supported by the similar spatial pattern between OC_{terr} and non-modern OC loadings, with higher values near riverine deltas and in the fine-grained mud areas (Fig. S13). However, elevated sedimentary non-modern OC loadings span more extensive regions, especially in central BS and southern YS (Fig. S13). The latter likely reflects the combined effects of supply of $OC_{pre\text{-}aged}$ delivered by Yellow River as well as aging during lateral sediment transport and associated hydrodynamic sorting (Bao et al., 2016, 2018b; Tao et al., 2016), resulting in widespread and enhanced potential burial of refractory OC in BS-YS sediments. OC aging decreases $\Delta^{14}C$ values but does not necessarily change the $\delta^{13}C$ values (Marwick et al., 2015), potentially influencing the source apportionment results. Thus, multiple approaches are needed to better constrain the fate of terrestrial OC pools in marine sediments (Belicka and Harvey, 2009; Blair and Aller, 2012; Zhu et al., 2013).

Our results also revealed a counterintuitive finding, i.e., the burial potential of OC_{fossil} is lower than that of $OC_{pre\text{-}aged}$, as indicated by increasing sedimentary $OC_{pre\text{-}aged}$ loadings and decreasing OC_{fossil} loadings relative to those of from the corresponding fluvial source inputs (Fig. 6 and Fig. S12). Tao et al. (2016) first made this observation based on a more limited dataset using a mass-balance OC budget approach, while our spatially-resolved data reveals that this is likely a pervasive phenomenon in BS-YS sediments. Based on the assumption of ~100% burial efficiency of soil pre-aged OC from the Yellow River and using biomarker mass balance, Sun et al. (2018) estimated that 58% of OC_{fossil} was lost before burial in a localized area of the Yellow River mouth, and suggested a portion of the OC_{fossil} loss could be due to microbial degradation. Decreasing OC_{fossil} loadings have also been observed along the coastal transport pathway (Fig. S14), which has also been recognized in the Mackenzie River-Beaufort shelf dispersal system (Goñi et al., 2005). In contrast, the higher sedimentary $OC_{pre\text{-}aged}$ loadings than riverine SPM implies contributions from additional $OC_{pre\text{-}aged}$ sources as well as stronger association with (and protection by) mineral surfaces than OC_{fossil} (Fig. 6). Thus, the contrasting fates of $OC_{pre\text{-}aged}$ and OC_{fossil} imply that age is not the only factor for OC burial potential but mineral associations, mineralogical composition (Blattmann et al., 2019) and sorting effect must also play a role.

The loadings of different terrestrial OC pools reveal spatial variability but many samples have much higher corresponding loadings than riverine samples. Uncertainties in source apportionment, mineral associations and composition, temporal variability in riverine loadings, as well as supply of terrestrial organic matter from other sources could be contributing factors. For example, OC pool loadings in marine sediments would reflect longer-term (decadal to centennial) averages, while data available for Yellow River SPM reflects a recent "snapshot". Although data for Yellow River SPM and biomarker-isotope loadings span only a three-year time series (Fig. 6; Yu et al., 2019a), they provide some insight into temporal variability in fluvial export. Moreover, the similar OC loadings for the middle reach (0.17 ± 0.04 mg C m^{-2}) and the lower reach (0.16 ± 0.04 mg C m^{-2}) SPM show that the Loess Plateau is the dominant sediment source to Yellow River SPM (Yu et al., 2019a; Qu et al., 2020). This has likely been the case for thousands of years, implying that OC loadings of SPM exported by the Yellow River would have remained similar over long time scales despite the large changes in sediment flux since 1950s (Wang et al., 2007). Nevertheless, while the Yellow River has historically been the dominant source of sediment and OC to the BS-YS, changes in the OC composition and transport dynamics caused by natural and anthropogenic activities (Zhang et al., 2013; Wang et al., 2017; Yu et al., 2019a, 2019b) may introduce uncertainty (Hilton et al., 2015). The recent diminishment in sediment supply may have caused other OC sources, such as from small rivers and atmospheric deposition, to have assumed greater prominence (Matsumoto et al., 2001; Tao et al., 2016), potentially resulting in higher $OC_{pre\text{-}aged}$ loadings. Sedimentation rates in the BS-YS have been relatively stable on centennial timescales (Hu et al., 2016; Qiao et al., 2017). However, spatial variability in sediment accumulation rates and mixed layer depths throughout the BS-YS (Qiao et al., 2017) imply that surficial sediments integrate supply over different time periods, potentially also contributing to the spatial variability in surface sediments.

The hydrodynamic setting can play an important role in the distribution and burial of OC (Hilton et al., 2011; Bao et al., 2018b; Hage et al., 2020), and is likely an important factor contributing to the spatial variability in terrestrially-derived OC pools in China marginal sea sediments. Relatively weak hydrodynamic conditions in the BS-YS (e.g., cold-water mass in southern YS) likely contribute to higher OC preservation (Hu et al., 2011, 2016; Zhao et al., 2018). This contrasts with the Yangtze River-ECS system and Pearl River-northern SCS system, which are characterized

by significant loss of OC_{terr} and lower burial efficiency (Wu et al., 2013; Hou et al., 2020). Higher OC loadings and fresher, more labile OC exported by the Yangtze River and Pearl River likely results in extensive degradation during transport and sedimentation, especially under stronger hydrodynamic settings (Wu et al., 2018; Lin et al., 2019; Wei et al., 2020). Similarly, physical reworking of sediments in the mobile-mud area in Yangtze River delta and ECS inner shelf enhances oxygen exposure time and OC remineralization (Blair and Aller, 2012; Wu et al., 2013; Xu et al., 2015; Zhao et al., 2018). Furthermore, the different mineralogical compositions of the Yellow, Yangtze and Pearl River SPM may also influence preservation of OC in shelf sediments (Zhu et al., 2013; Blattmann et al., 2019; Hemingway et al., 2019).

These findings underscore the need for further investigation of the mechanisms controlling the fates of different terrestrial OC pools among different river-dominated margin systems, and for assessments of the effects of climate and anthropogenic perturbations on OC supply and burial. Improved characterization and quantification of terrestrial OC fractions in marine sediments requires application of different proxies and approaches (e.g., Belicka and Harvey, 2009; Blair and Aller, 2012; Zhu et al., 2013). Such investigations should be extended to other hotspots of carbon burial (e.g., continental slopes, fjords, deep-sea fans and deep-ocean trenches) in order to refine assessments of terrestrial OC burial in the global ocean (Burdige, 2005; Smith et al., 2015; Hage et al., 2020; Xiao et al., 2020).

5. CONCLUSION

This study used bulk and molecular-level $\delta^{13}C$ and $\Delta^{14}C$ measurements to assess spatial variations in the composition, age and burial potential of different terrestrial OC pools in BS-YS sediments. The results reveal significant spatial variability in the fractional abundance of OC_{terr} and of different aged OC pools. On average, OC_{modern}, $OC_{pre\text{-}aged}$ and OC_{fossil} accounted for 49 ± 10%, 37 ± 6% and 13 ± 6% of TOC, respectively. The average contribution of non-modern OC ($OC_{pre\text{-}aged}$ and OC_{fossil}; 51 ± 10%) was broadly equal to that of OC_{terr} estimated from $\delta^{13}C_{OC}$ (ave., 51 ± 14%), implying that OC_{terr} in BS-YS is mainly composed of millennial-aged OC. Since sedimentary TOC and sub-OC pools in BS-YS all exhibited strong association with mineral surfaces, we constrained fates of different terrestrial OC pools by contrasting mineral SA-normalized OC loadings of sediments to those of corresponding Yellow River POC. Both the regression slope-derived mean value and the arithmetic mean value of loadings revealed efficient sequestration of all terrestrial OC pools in BS-YS sediments. The similar proto-burial patterns of OC_{terr} and non-modern OC suggest high burial potential of predominantly millennial-aged OC exported by the Yellow River. The extensive dataset also reveals contrasting fates of $OC_{pre\text{-}aged}$ and OC_{fossil}. Specifically, increased sedimentary $OC_{pre\text{-}aged}$ loadings and decreased OC_{fossil} loadings relative to those of fluvial inputs suggest consistently higher burial potential of $OC_{pre\text{-}aged}$ than OC_{fossil}, implying enhanced degradation of OC_{fossil} during transport, different mineral associations and sorting effects, and/or additional $OC_{pre\text{-}aged}$ sources. Elucidation of underlying causes requires further research.

The uniformly high burial potential of terrestrial OC in the BS-YS is attributed to the refractory nature of OC transported by the Yellow River that, in turn, is a consequence of its antiquity and close mineral association. Sediment transport and deposition processes likely contribute to spatial variations in OC proto-burial patterns. Thus, diverse OC inputs, mineralogical compositions and hydrological settings influence the fates of terrestrial OC in China marginal seas. Our study highlights the need for detailed characterization of specific terrestrial OC pools in different river-marginal sea systems in order to refine our understanding of the fate of terrestrial OC exported to the ocean, and evaluate the influence of natural and anthropogenic processes on OC cycling.

Declaration of Competing Interest

The authors declare that they have no known competing financial interests or personal relationships that could have appeared to influence the work reported in this paper.

ACKNOWLEDGEMENTS

We thank Dr. Jordon Hemingway for the constructive suggestions on the manuscript and Dr. Limin Hu for discussions. We are grateful to Editor-in-Chief Prof. Jeffrey G. Catalano and Associate Editor Prof. Elizabeth A. Canuel for handling the manuscript and valuable suggestions, and three anonymous reviewers for their thoughtful and valuable comments that help improve the manuscript. We would like to thank Qiang Liu, Weijie Hao, the crews of *R/V Dongfanghong II* for sampling help, Hailong Zhang, Li Li and Gui'e Jin for laboratory assistance. We also thank all members of Laboratory for Ion Beam Physics at ETH Zürich for ^{14}C measurements. This study was supported by the National Key Research and Development Program of China (M. Z., Grant No. 2016YFA0601403), the National Natural Science Foundation of China (M. Z., Grant Nos. 41630966, U1706219; M. Y., 41906032), the Swiss National Science Foundation (T. E., "CAPS-LOCK2" Grant #200020_163162, "CAPS-LOCK3" Grant #200020_184865), the "111" Project (B13030), and the China Scholarship Council (M. Y., No. 201506330021). This is MCTL (Key Laboratory of Marine Chemistry Theory and Technology) contribution #218.

APPENDIX A. SUPPLEMENTARY MATERIAL

Supplementary data to this article can be found online at https://doi.org/10.1016/j.gca.2021.06.018.

REFERENCES

Andersson A., Deng J., Du K., Zheng M., Yan C., Sköld M. and Gustafsson Ö. (2015) Regionally-varying combustion sources of the January 2013 severe haze events over eastern China. *Environ. Sci. Technol.* **49**, 2038–2043.

Aller R. C., Blair N. E. and Brunskill G. J. (2008) Early diagenetic cycling, incineration, and burial of sedimentary organic carbon

in the central Gulf of Papua (Papua New Guinea). *J. Geophys. Res.* **113**, F01S09.

Bao R., McIntyre C., Zhao M., Zhu C., Kao S. J. and Eglinton T. I. (2016) Widespread dispersal and aging of organic carbon in shallow marginal seas. *Geology* **44**, 791–794.

Bao R., Uchida M., Zhao M., Haghipour N., Montlucon D., McNichol A., Wacker L., Hayes J. M. and Eglinton T. I. (2018a) Organic carbon aging during across-shelf transport. *Geophys. Res. Lett.* **45**, 8425–8434.

Bao R., van der Voort T. S., Zhao M., Guo X., Montluçon D. B., McIntyre C. and Eglinton T. I. (2018b) Influence of hydrodynamic processes on the fate of sedimentary organic matter on continental margins. *Global Biogeochem. Cycles* **32**, 1420–1432.

Bao R., Zhao M., McNichol A. P., Wu Y., Guo X., Haghipour N. and Eglinton T. I. (2019) On the origin of aged sedimentary organic matter along a river-shelf-deep ocean transect. *J. Geophys. Res.-Biogeosciences* **124**.

Bauer J. E., Cai W.-J., Raymond P. A., Bianchi T. S., Hopkinson C. S. and Regnier P. A. (2013) The changing carbon cycle of the coastal ocean. *Nature* **504**, 61–70.

Belicka L. L. and Harvey H. R. (2009) The sequestration of terrestrial organic carbon in Arctic Ocean sediments: a comparison of methods and implications for regional carbon budgets. *Geochim. Cosmochim. Acta* **73**, 6231–6248.

Bianchi T. S., Cui X., Blair N. E., Burdige D. J., Eglinton T. I. and Galy V. (2018) Centers of organic carbon burial and oxidation at the land-ocean interface. *Org. Geochem.* **115**, 138–155.

Blair N. E. and Aller R. C. (2012) The fate of terrestrial organic carbon in the marine environment. *Annu. Rev. Mar. Sci* **4**, 401–423.

Blattmann T. M., Liu Z., Zhang Y., Zhao Y., Haghipour N., Montluçon D. B., Plötze M. and Eglinton T. I. (2019) Mineralogical control on the fate of continentally derived organic matter in the ocean. *Science*, eaax5345.

Bröder L., Tesi T., Salvadó J. A., Semiletov I. P., Dudarev O. V. and Gustafsson Ö. (2016) Fate of terrigenous organic matter across the Laptev Sea from the mouth of the Lena River to the deep sea of the Arctic interior. *Biogeosciences* **13**, 5003–5019.

Bröder L., Tesi T., Andersson A., Semiletov I. and Gustafsson Ö. (2018) Bounding cross-shelf transport time and degradation in Siberian-Arctic land-ocean carbon transfer. *Nat. Commun.* **9**, 806.

Burdige D. J. (2005) Burial of terrestrial organic matter in marine sediments: a re-assessment. *Global Biogeochem. Cycles* **19**, GB4011.

Butman D. E., Wilson H. F., Barnes R. T., Xenopoulos M. A. and Raymond P. A. (2015) Increased mobilization of aged carbon to rivers by human disturbance. *Nat. Geosci.* **8**, 112–116.

Christl M., Vockenhuber C., Kubik P. W., Wacker L., Lachner J., Alfimov V. and Synal H. A. (2013) The ETH Zurich AMS facilities: performance parameters and reference materials. *Nucl. Instrum. Methods Phys. Res., Sect. B* **294**, 29–38.

Collister J. W., Rieley G., Stern B., Eglinton G. and Fry B. (1994) Compound-specific $\delta^{13}C$ analyses of leaf lipids from plants with differing carbon dioxide metabolisms. *Org. Geochem.* **21**, 619–627.

Deng B., Zhang J. and Wu Y. (2006) Recent sediment accumulation and carbon burial in the East China Sea. *Global Biogeochem. Cycles* **20**, GB3014.

Drenzek N. J., Montluçon D. B., Yunker M. B., Macdonald R. W. and Eglinton T. I. (2007) Constraints on the origin of sedimentary organic carbon in the Beaufort Sea from coupled molecular ^{13}C and ^{14}C measurements. *Mar. Chem.* **103**, 146–162.

Eglinton T. I., Benitez-Nelson B. C., Pearson A., McNichol A. P., Bauer J. E. and Druffel E. R. M. (1997) Variability in radiocarbon ages of individual organic compounds from marine sediments. *Science* **277**, 796–799.

Feng X., Benitez-Nelson B. C., Montluçon D. B., Prahl F. G., McNichol A. P., Xu L., Repeta D. J. and Eglinton T. I. (2013) ^{14}C and ^{13}C characteristics of higher plant biomarkers in Washington margin surface sediments. *Geochim. Cosmochim. Acta* **105**, 14–30.

French K. L., Hein C. J., Haghipour N., Wacker L., Kudrass H. R., Eglinton T. I. and Galy V. (2018) Millennial soil retention of terrestrial organic matter deposited in the Bengal Fan. *Sci. Rep.* **8**, 11997.

Freymond C. V., Kündig N., Stark C., Peterse F., Buggle B., Lupker M., Plötze M., Blattmann T. M., Filip F., Giosan L. and Eglinton T. I. (2018) Evolution of biomolecular loadings along a major river system. *Geochim. Cosmochim. Acta* **223**, 389–404.

Fry B. and Sherr E. B. (1984) $\delta^{13}C$ measurements as indicators of carbon flow in marine and freshwater ecosystems. *Mar. Sci.* **27**, 13–47.

Galy V., France-Lanord C., Beyssac O., Faure P., Kudrass H. and Palhol F. (2007) Efficient organic carbon burial in the Bengal fan sustained by the Himalayan erosional system. *Nature* **450**, 407–410.

Galy V., Peucker-Ehrenbrink B. and Eglinton T. (2015) Global carbon export from the terrestrial biosphere controlled by erosion. *Nature* **521**, 204–207.

Goñi M. A., Yunker M. B., Macdonald R. W. and Eglinton T. I. (2005) The supply and preservation of ancient and modern components of organic carbon in the Canadian Beaufort Shelf of the Arctic Ocean. *Mar. Chem.* **93**, 53–73.

Griffith D. R., Martin W. R. and Eglinton T. I. (2010) The radiocarbon age of organic carbon in marine surface sediments. *Geochim. Cosmochim. Acta* **74**, 6788–6800.

Hage S., Galy V. V., Cartigny M. J. B., Acikalin S., Clare M. A., Gröcke D. R., Hilton R. G., Hunt J. E., Lintern D. G., McGhee C. A., Parsons D. R., Stacey C. D., Sumner E. J. and Talling P. J. (2020) Efficient preservation of young terrestrial organic carbon in sandy turbidity-current deposits. *Geology* **48**.

Hedges J. I. and Keil R. G. (1995) Sedimentary organic matter preservation: an assessment and speculative synthesis. *Mar. Chem.* **49**, 81–115.

Hemingway J. D., Rothman D. H., Grant K. E., Rosengard S. Z., Eglinton T. I., Derry L. A. and Galy V. V. (2019) Mineral protection regulates long-term global preservation of natural organic carbon. *Nature* **570**, 228–231.

Hilton R. G., Galy A., Hovius N., Horng M. J. and Chen H. (2011) Efficient transport of fossil organic carbon to the ocean by steep mountain rivers: an orogenic carbon sequestration mechanism. *Geology* **39**, 71–74.

Hilton R. G., Galy V., Gaillardet J., Dellinger M., Bryant C., O'Regan M., Grocke D. R., Coxall H., Bouchez J. and Calmels D. (2015) Erosion of organic carbon in the Arctic as a geological carbon dioxide sink. *Nature* **524**, 84–87.

Hou P., Yu M., Zhao M., Montluçon D. B., Su C. and Eglinton T. I. (2020) Terrestrial biomolecular burial efficiencies on continental margins. *J. Geophys. Res. Biogeosciences* **125**, e2019JG005520.

Hu L., Shi X., Bai Y., Qiao S., Li L., Yu Y., Yang G., Ma D. and Guo Z. (2016) Recent organic carbon sequestration in the shelf sediments of the Bohai Sea and Yellow Sea, China. *J. Mar. Syst.* **155**, 50–58.

Hu L. M., Lin T., Shi X. F., Yang Z. S., Wang H. J., Zhang G. and Guo Z. G. (2011) The role of shelf mud depositional process and large river inputs on the fate of organochlorine pesticides in sediments of the Yellow and East China seas. *Geophys. Res. Lett.* **38**.

Kang S., Kim J. H., Ryu J. S. and Shin K. H. (2020) Dual carbon isotope ($\delta^{13}C$ and $\Delta^{14}C$) characterization of particulate organic carbon in the Geum and Seomjin estuaries, South Korea. *Mar. Pollut. Bull.* **150** 110719.

Keil R. G., Tsamakis E., Fuh C. B., Giddings J. C. and Hedges J. I. (1994) Mineralogical and textural controls on the organic composition of coastal marine sediments: hydrodynamic separation using SPLITT-fractionation. *Geochim. Cosmochim. Acta* **58**, 879–893.

Keil R. G., Mayer L. M., Quay P. D., Richey J. E. and Hedges J. I. (1997) Loss of organic matter from riverine particles in deltas. *Geochim. Cosmochim. Acta* **61**, 1507–1511.

Komada T., Anderson M. R. and Dorfmeier C. L. (2008) Carbonate removal from coastal sediments for the determination of organic carbon and its isotopic signatures, $\delta^{13}C$ and $\Delta^{14}C$: comparison of fumigation and direct acidification by hydrochloric acid. *Limnol. Oceanogr. Methods* **6**, 254–262.

Lamb A. L., Wilson G. P. and Leng M. J. (2006) A review of coastal palaeoclimate and relative sea-level reconstructions using $\delta^{13}C$ and C/N ratios in organic material. *Earth-Sci. Rev.* **75**, 29–57.

Leithold E. L., Blair N. E. and Wegmann K. W. (2016) Source-to-sink sedimentary systems and global carbon burial: a river runs through it. *Earth-Sci. Rev.* **153**, 30–42.

Lin B., Liu Z., Eglinton T. I., Kandasamy S., Blattmann T. M., Haghipour N. and de Lange G. J. (2019) Perspectives on provenance and alteration of suspended and sedimentary organic matter in the subtropical Pearl River system, South China. *Geochim. Cosmochim. Acta*.

Liu D., Li X., Emeis K.-C., Wang Y. and Richard P. (2015) Distribution and sources of organic matter in surface sediments of Bohai Sea near the Yellow River Estuary, China. *Estuar. Coast. Shelf Sci.* **165**, 128–136.

Liu W., An Z., Zhou W., Head M. J. and Cai D. (2003) Carbon isotope and C/N ratios of suspended matter in rivers: an indicator of seasonal change in C4/C3 vegetation. *Appl. Geochem.* **18**, 1241–1249.

Liu W., Yang H., Ning Y. and An Z. (2007) Contribution of inherent organic carbon to the bulk $\delta^{13}C$ signal in loess deposits from the arid western Chinese Loess Plateau. *Org. Geochem.* **38**, 1571–1579.

Marwick T. R., Tamooh F., Teodoru C. R., Borges A. V., Darchambeau F. and Bouillon S. (2015) The age of river-transported carbon: a global perspective. *Global Biogeochem. Cycles* **29**, 122–137.

Matsumoto K., Kawamura K., Uchida M., Shibata Y. and Yoneda M. (2001) Compound specific radiocarbon and $\delta^{13}C$ measurements of fatty acids in a continental aerosol sample. *Geophys. Res. Lett.* **28**, 4587–4590.

Mayer L. M. (1994a) Surface area control of organic carbon accumulation in continental shelf sediments. *Geochim. Cosmochim. Acta* **58**, 1271–1284.

Mayer L. M. (1994b) Relationships between mineral surfaces and organic carbon concentrations in soils and sediments. *Chem. Geol.* **114**, 347–363.

McIntyre C. P., Wacker L., Haghipour N., Blattmann T. M., Fahrni S., Usman M., Eglinton T. I. and Synal H.-A. (2017) Online ^{13}C and ^{14}C gas measurements by EA-IRMS–AMS at ETH Zürich. *Radiocarbon* **59**, 893–903.

Qi L., Wu Y., Chen S. and Wang X. (2021) Evaluation of abandoned Huanghe Delta as an important carbon source for the Chinese marginal seas in recent decades. *J. Geophys. Res. Oceans* **126**, e2020JC017125.

Qiao S., Shi X., Wang G., Zhou L., Hu B., Hu L., Yang G., Liu Y., Yao Z. and Liu S. (2017) Sediment accumulation and budget in the Bohai Sea, Yellow Sea and East China Sea. *Mar. Geol.* **390**, 270–281.

Qu Y., Jin Z., Wang J., Wang Y., Xiao J., Gou L.-F., Zhang F., Liu C.-Y., Gao Y., Suarez M. B. and Xu X. (2020) The sources and seasonal fluxes of particulate organic carbon in the Yellow River. *Earth Surf. Process. Landforms* **45**, 2004–2019.

Regnier P., Friedlingstein P., Ciais P., Mackenzie F. T., Gruber N., Janssens I. A., Laruelle G. G., Lauerwald R., Luyssaert S., Andersson A. J., Arndt S., Arnosti C., Borges A. V., Dale A. W., Gallego-Sala A., Goddéris Y., Goossens N., Hartmann J., Heinze C., Ilyina T., Joos F., LaRowe D. E., Leifeld J., Meysman F. J. R., Munhoven G., Raymond P. A., Spahni R., Suntharalingam P. and Thullner M. (2013) Anthropogenic perturbation of the carbon fluxes from land to ocean. *Nat. Geosci.* **6**, 597–607.

Schlitzer, R. (2018). Ocean Data View. Available on https://odv.awi.de/.

Schouten S., Klein Breteler W. C. M., Blokker P., Schogt N., Rijpstra W. I. C., Grice K., Baas M. and Sinninghe Damsté J. S. (1998) Biosynthetic effects on the stable carbon isotopic compositions of algal lipids: implications for deciphering the carbon isotopic biomarker record. *Geochim. Cosmochim. Acta* **62**, 1397–1406.

Smith R. W., Bianchi T. S., Allison M., Savage C. and Galy V. (2015) High rates of organic carbon burial in fjord sediments globally. *Nat. Geosci.* **8**, 450–453.

Sun D., Tang J., He Y., Liao W. and Sun Y. (2018) Sources, distributions, and burial efficiency of terrigenous organic matter in surface sediments from the Yellow River mouth, northeast China. *Org. Geochem.* **118**, 89–102.

Tao S., Eglinton T. I., Montluçon D. B., McIntyre C. and Zhao M. (2015) Pre-aged soil organic carbon as a major component of the Yellow River suspended load: Regional significance and global relevance. *Earth Planet. Sci. Lett.* **414**, 77–86.

Tao S., Eglinton T. I., Montluçon D. B., McIntyre C. and Zhao M. (2016) Diverse origins and pre-depositional histories of organic matter in contemporary Chinese marginal sea sediments. *Geochim. Cosmochim. Acta* **191**, 70–88.

Tao S., Eglinton T. I., Zhang L., Yi Z., Montluçon D. B., McIntyre C., Yu M. and Zhao M. (2018) Temporal variability in composition and fluxes of Yellow River particulate organic matter. *Limnol. Oceanogr.* **63**, S119–S141.

Tesi T., Semiletov I., Hugelius G., Dudarev O., Kuhry P. and Gustafsson Ö. (2014) Composition and fate of terrigenous organic matter along the Arctic land–ocean continuum in East Siberia: insights from biomarkers and carbon isotopes. *Geochim. Cosmochim. Acta* **133**, 235–256.

Tesi T., Semiletov I., Dudarev O., Andersson A. and Gustafsson Ö. (2016) Matrix association effects on hydrodynamic sorting and degradation of terrestrial organic matter during cross-shelf transport in the Laptev and East Siberian shelf seas. *J. Geophys. Res. Biogeosciences* **121**, 731–752.

van der Voort T. S., Mannu U., Blattmann T. M., Bao R., Zhao M. and Eglinton T. I. (2018) Deconvolving the fate of carbon in coastal sediments. *Geophys. Res. Lett.* **45**, 4134–4142.

Vonk J. E., Sanchez-Garcia L., Semiletov I. P., Dudarev O. V., Eglinton T. I., Andersson A. and Gustafsson O. (2010) Molecular and radiocarbon constraints on sources and degradation of terrestrial organic carbon along the Kolyma paleoriver transect, East Siberian Sea. *Biogeosciences* **7**, 3153–3166.

Vonk J. E., Giosan L., Blusztajn J., Montlucon D., Graf Pannatier E., McIntyre C., Wacker L., Macdonald R. W., Yunker M. B. and Eglinton T. I. (2015) Spatial variations in geochemical characteristics of the modern Mackenzie Delta sedimentary system. *Geochim. Cosmochim. Acta* **171**, 100–120.

Vonk J. E., Drenzek N. J., Hughen K. A., Stanley R. H. R., McIntyre C., Montluçon D. B., Giosan L., Southon J. R., Santos G. M., Druffel E. R. M., Andersson A. A., Sköld M. and Eglinton T. I. (2019) Temporal deconvolution of vascular plant-derived fatty acids exported from terrestrial watersheds. *Geochim. Cosmochim. Acta* **244**, 502–521.

Wakeham S. G., Canuel E. A., Lerberg E. J., Mason P., Sampere T. P. and Bianchi T. S. (2009) Partitioning of organic matter in continental margin sediments among density fractions. *Mar. Chem.* **115**, 211–225.

Wang H., Wu X., Bi N., Li S., Yuan P., Wang A., Syvitski J. P. M., Saito Y., Yang Z., Liu S. and Nittrouer J. (2017) Impacts of the dam-orientated water-sediment regulation scheme on the lower reaches and delta of the Yellow River (Huanghe): a review. *Global Planet. Change* **157**, 93–113.

Wang H., Yang Z., Saito Y., Liu J. P., Sun X. and Wang Y. (2007) Stepwise decreases of the Huanghe (Yellow River) sediment load (1950–2005): Impacts of climate change and human activities. *Global Planet. Change* **57**, 331–354.

Wang X., Ma H., Li R., Song Z. and Wu J. (2012) Seasonal fluxes and source variation of organic carbon transported by two major Chinese Rivers: the Yellow River and Changjiang (Yangtze) River. *Global Biogeochem. Cycles* **26**, GB2025.

Wei B., Mollenhauer G., Hefter J., Grotheer H. and Jia G. (2020) Dispersal and aging of terrigenous organic matter in the Pearl River Estuary and the northern South China Sea Shelf. *Geochim. Cosmochim. Acta* **282**, 324–339.

Wu Y., Eglinton T., Yang L., Deng B., Montluçon D. and Zhang J. (2013) Spatial variability in the abundance, composition, and age of organic matter in surficial sediments of the East China Sea. *J. Geophys. Res. Biogeosciences* **118**, 1495–1507.

Wu Y., Eglinton T. I., Zhang J. and Montlucon D. B. (2018) Spatio-temporal variation of the quality, origin and age of particulate organic matter transported by the Yangtze River (Changjiang). *J. Geophys. Res. Biogeosciences* **123**, 2908–2921.

Xiao W., Xu Y., Haghipour N., Montlucon D., Pan B., Jia Z., Ge H., Yao P. and Eglinton T. I. (2020) Efficient sequestration of terrigenous organic carbon in the New Britain Trench. *Chem. Geol.* **533** 119466.

Xing L., Tao S., Zhang H., Liu Y., Yu Z. and Zhao M. (2011) Distributions and origins of lipid biomarkers in surface sediments from the southern Yellow Sea. *Appl. Geochem.* **26**, 1584–1593.

Xing L., Zhao M., Gao W., Wang F., Zhang H., Li L., Liu J. and Liu Y. (2014) Multiple proxy estimates of source and spatial variation in organic matter in surface sediments from the southern Yellow Sea. *Org. Geochem.* **76**, 72–81.

Xing L., Hou D., Wang X., Li L. and Zhao M. (2016) Assessment of the sources of sedimentary organic matter in the Bohai Sea and the northern Yellow Sea using biomarker proxies. *Estuar. Coast. Shelf Sci.* **176**, 67–75.

Xu B., Bianchi T. S., Allison M. A., Dimova N. T., Wang H., Zhang L., Diao S., Jiang X., Zhen Y., Yao P., Chen H., Yao Q., Dong W., Sui J. and Yu Z. (2015) Using multi-radiotracer techniques to better understand sedimentary dynamics of reworked muds in the Changjiang River estuary and inner shelf of East China Sea. *Mar. Geol.* **370**, 76–86.

Xue Y., Zou L., Ge T. and Wang X. (2017) Mobilization and export of millennial-aged organic carbon by the Yellow River. *Limnol. Oceanogr.* **62**, S95–S111.

Yang S. Y., Jung H. S., Lim D. and Li C. X. (2003) A review on the provenance discrimination of sediments in the Yellow Sea. *Earth-Sci. Rev.* **63**, 93–120.

Yoon S.-H., Kim J.-H., Yi H.-I., Yamamoto M., Gal J.-K., Kang S. and Shin K.-H. (2016) Source, composition and reactivity of sedimentary organic carbon in the river-dominated marginal seas: a study of the eastern Yellow Sea (the northwestern Pacific). *Cont. Shelf Res.* **125**, 114–126.

Yu M., Guo Z., Wang X., Eglinton T. I., Yuan Z., Xing L., Zhang H. and Zhao M. (2018a) Sources and radiocarbon ages of aerosol organic carbon along the east coast of China and implications for atmospheric fossil carbon contributions to China marginal seas. *Sci. Total Environ.* **619–620**, 957–965.

Yu M., Zhang H., Li L. and Zhao M. (2018b) Spatial Distributions and Potential Sources of Long Chain (C30, C32 1,15-) Alkyl Diols in Surface Sediments from Eastern China Marginal Seas. *J. Ocean Univ. Chin.* **17**, 1114–1122.

Yu M., Eglinton T. I., Haghipour N., Montlucon D., Wacker L., Hou P., Zhang H. and Zhao M. (2019a) Impacts of natural and human-induced hydrological variability on particulate organic carbon dynamics in the Yellow River. *Environ. Sci. Technol.* **53**, 1119–1129.

Yu M., Eglinton T. I., Haghipour N., Montluçon D. B., Wacker L., Wang Z., Jin G. E. and Zhao M. (2019b) Molecular isotopic insights into hydrodynamic controls on fluvial suspended particulate organic matter transport. *Geochim. Cosmochim. Acta* **262**, 78–91.

Zhang L. J., Wang L., Cai W. J., Liu D. M. and Yu Z. G. (2013) Impact of human activities on organic carbon transport in the Yellow River. *Biogeosciences* **10**, 2513–2524.

Zhao B., Yao P., Bianchi T. S., Arellano A. R., Wang X., Yang J., Su R., Wang J., Xu Y., Huang X., Chen L., Ye J. and Yu Z. (2018) The remineralization of sedimentary organic carbon in different sedimentary regimes of the Yellow and East China Seas. *Chem. Geol.* **495**, 104–117.

Zhou L., Liu J., Saito Y., Zhang Z., Chu H. and Hu G. (2014) Coastal erosion as a major sediment supplier to continental shelves: example from the abandoned Old Huanghe (Yellow River) delta. *Cont. Shelf Res.* **82**, 43–59.

Zhu C., Wagner T., Talbot H. M., Weijers J. W., Pan J.-M. and Pancost R. D. (2013) Mechanistic controls on diverse fates of terrestrial organic components in the East China Sea. *Geochim. Cosmochim. Acta* **117**, 129–143.

Associate editor: Elizabeth Ann Canuel